Annals of Biomedical Engineering, Vol. 30, pp. 1064–1076, 2002
Printed in the USA.

0090-6964/2002/30(8)/1064/13/$15.00

Model-Based Evaluation of Eustachian Tube Mechanical Properties Using Continuous Pressure–Flow Rate Data

SAMIR N. GHADIALI,[1,3] J. DOUGLAS SWARTS,[3] and WILLIAM J. FEDERSPIEL[1,2]

[1]Department of Chemical Engineering, [2]Department of Surgery and Bioengineering, and [3]Department of Pediatric Otolaryngology, Children's Hospital of Pittsburgh, Pittsburgh, PA

(Received 10 August 2001; accepted 16 July 2002)

Abstract—Eustachian tube (ET) dysfunction has been implicated in the development of chronic otitis media, a common childhood disorder. An impaired ability to open the collapsible ET results in fluid accumulation in the middle ear and subsequent infection and inflamation. Abnormal ET function has been casually related to an abnormal mechanical environment. Previous attempts to quantify ET mechanics used summary measures that are not clearly related to the physical properties of the system. In this study, we modified a testing technique to obtain pressure and flow rate measurements in the ET and analyzed these data with a simple model of airflow in a collapsible tube. This model is based on fully developed flow in a noncircular duct and a nonlinear, time-dependent pressure–area relationship. The ability of this model to capture the observed pressure–flow phenomena was demonstrated in 12 cynomolgus monkeys. Correlation between model and experimental data resulted in quantitative estimates of ET compliance and wall viscosity. This technique, which can be implemented in a clinical setting, provides a more accurate description of ET mechanics and may, therefore, prove to be an important diagnostic tool. Future studies will use this technique to quantify the influence of various physiological parameters on ET mechanics.

[DOI: 10.1114/1.1509764]

Keywords—Collapsible tubes, Biologic systems, Compliance, Elasticity, Viscoelasticity, Fluid-structure models, Tube law.

INTRODUCTION

Otitis media (OM) is an infectious disease that generally includes inflammation of the middle ear (ME) mucosa and an accumulation of fluid within the ME space. A 1990 survey by the Centers for Disease Control (CDC) identified 24.5 million physician office visits at which the primary diagnosis was OM.[26] By age three, a significant number of children (33%) experience >3 episodes of OM (chronic OM).[32] The CDC survey also indicated that 20% of all physician visits were by patients 15 years of age and older. Chronic OM, therefore, affects a large portion of the population. Although bacterial or viral infections and nasal allergies contribute to the onset of OM, the development of chronic OM is associated with the functional impairment of the eustachian tube.[6]

The eustachian tube (ET) is a collapsible structure which connects the ME space with the nasal cavity. The structure of the ET is similar to other respiratory airways in that the lumen of the tube contains a fluid layer, the mucosa, and is surrounded by cartilaginous and muscular elements.[6] The most important functions of the ET include (1) protection of the ME from pathogens of the nasopharynx, (2) pressure regulation or ventilation to equilibrate the ME with atmospheric pressure, and (3) drainage and/or clearance of fluid which has accumulated in the ME into the nasopharynx.[5] Under normal conditions, the ET exists in a collapsed ''closed'' configuration which protects the ME from nasopharyngeal secretions. The ventilation and clearance functions, however, require an open ET in which the resistance to air and fluid flow is minimal. Optimal function, therefore, only occurs when the ET opens intermittently due to the contraction of the surrounding musculature.

The inability of the ET to perform these physiological functions may be due to an abnormal mechanical environment. Several investigators[16,21,30] have specifically suggested that ET function may depend on the tube's compliance (or elasticity). The compliance of the ET can affect both the ability to open the tube (distensibility) and the ability to close the tube once it is opened (collapsibility).[21] Rigid or inelastic ETs (low compliance) are difficult to open and thus might impair the ventilation and clearance functions. Once a rigid tube is opened, its inelastic nature may also prevent it from closing, resulting in a patulous ET that impairs the protective function. Conversely, ETs with high compliance, often known as ''floppy'' ETs,[5] may impair both the protective and clearance functions by opening and collapsing too easily. This lack of stiffness may also affect the ability of the surrounding musculature to actively open the tube during

Address correspondence to Samir N. Ghadiali, PhD, Department of Pediatric Otolaryngology, Children's Hospital of Pittsburgh, Rm 8152, Rangos Research Center, 3460 Fifth Ave, Pittsburgh, PA 15213. Electronic mail: ghadiali@pitt.edu

swallowing. Normal ET function may, therefore, depend on optimal mechanical properties.

Several simple methods of evaluating ET function can be performed on an intact tympanic membrane (TM), but more biomechanically informative tests (such as the forced-response test described below) require a perforated TM. These tests are most often used on individuals whose treatment would include a surgical opening of the TM (myringotomy). Myringotomies are typically performed on patients who do not respond to antimicrobial agents and have displayed OM-related symptoms for >3–6 months.[5] These individuals may have abnormal ET function and, consequently, are at risk for developing chronic OM. Therefore, a diagnostic test that can quantify this risk by accurately measuring the mechanical properties (such as compliance) of the ET is desirable.

Currently, two different clinical methods of measuring ET compliance have been reported.[15,29] The first uses pressure and volume data from a balloon introduced into the ET lumen. Due to the relative invasiveness of balloon insertion and the unknown effects of the balloon on tubal geometry and mechanics, few research groups have adopted this method. The second method, however, is significantly less invasive and uses pressure and flow data acquired during the standard forced-response test.[8] In this test, the ET is opened via inflation of the ME and airflow is continued until a steady-state pressure and flow rate is achieved. This test can measure several intrinsic properties such as the pressure required to open the tube, the passive resistance to air flow at steady state, and the active resistance during swallowing, but it is difficult to directly measure specific biomechanical properties such as compliance. Takahashi and colleagues[21,29,30] attempted to quantify ET compliance using a summary parameter known as the tubal compliance index (TCI), which is a ratio of passive resistance at two separate flow rates. The TCI, however, may not be an accurate measure since it is acquired using a limited data set (i.e., pressure measurement at two distinct flow rates) and does not measure the ''true'' engineering compliance, which is defined as the change in tube area in response to changes in the applied pressure. Although the ET's cross-sectional area is not easy to measure, previous investigations of other collapsible biological tubes, such as arteries and the urethra, have demonstrated that compliance information can be extracted from continuous pressure–flow rate measurements.[2,9,17]

The goal of the present study is to use similar engineering principles to develop a diagnostic testing method which can accurately determine ET mechanical properties. Specifically, we have modified the current clinical test in order to obtain continuous, oscillatory pressure–flow rate measurements. The mechanical properties (compliance and wall viscosity) will be determined by analyzing these pressure–flow data with a simple fluid-structure model of airflow in the ET. Determination of these mechanical properties may lead to a better understanding and diagnosis of the factors responsible for the development of chronic OM.

FLUID-STRUCTURE MODELS

Airflow in the ET is governed by the incompressible Navier–Stokes and continuity equations,

$$\rho\left(\frac{\partial \mathbf{u}}{\partial t}+(\mathbf{u}\cdot\nabla)\mathbf{u}\right)=-\nabla p+\mu\nabla^2\mathbf{u} \quad \text{and} \quad \nabla\cdot\mathbf{u}=0, \tag{1}$$

where p represents the fluid pressure, $\mathbf{u}$ is the three-dimensional velocity vector, ρ is the density of air, and μ is the viscosity of air. The solution to these equations, which specify conservation of momentum and mass in the fluid, will depend on the local geometry of the collapsible tube. Deformation of the tube due to fluid stresses and pressures will, however, alter the local geometry. The structural mechanics of this deformation will be governed by a generalized ''tube law,''

$$\Delta p=p_{\text{int}}-p_{\text{ext}}=\tilde{P}(A), \tag{2}$$

which relates the transmural pressure (internal–external), Δp, across the tube wall with the local cross-sectional area, A, and potentially the time derivative of A. The solution of Eq. (2) for the local geometry, A, requires knowledge of the fluid pressure, p, and the solution of Eq. (1) for p and $\mathbf{u}$ requires knowledge of A. A complete analysis of flow in a collapsible tube would, therefore, require a complex solution algorithm that can account for this fluid-structure coupling. Although several investigators[11,13,14,18,19,23] have performed this detailed analysis using boundary-element, finite-element, and finite-difference methods, our goal is to develop a relatively simple fluid-structure model that can be used in a clinical setting. This model, which is based on several simplifying assumptions, will generate solutions that can be readily correlated with experimental pressure–flow measurements to determine ET mechanical properties.

Figure 1 shows a diagram of the simple fluid-structure model to be analyzed in this study. The collapsible segment of the ET is supported by elastic (E) and viscous (μ_w) elements. The mean pressure within the tube must exceed the external periluminal pressure (p_{ext}) in order to obtain a nonzero cross-sectional area (A). Although Fig. 1 depicts an axisymmetric circular cross section, the model equations will be developed for an arbitrary cross-sectional geometry, which maintains its general configuration as the area changes. Once opened, the airflow through the tube (Q) is governed by the pressure differ-

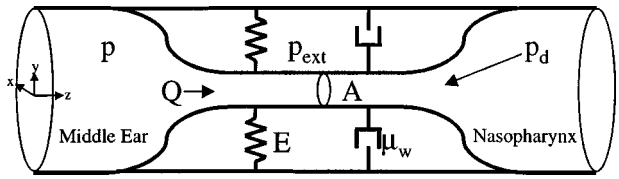

FIGURE 1. Simple fluid-structure model of airflow in a collapsed tube where the tube wall is supported by elastic (*E*) and viscous (μ_w) elements.

ence between the upstream ME pressure (p) and downstream nasopharyngeal pressure (p_d). As described in the Methods section, the experiments will involve prescribing an oscillatory flow rate with a frequency ω and measuring the resulting oscillations in the upstream pressure. The upstream pressure and flow rate will, therefore, be functions of time, i.e., $p=p(t)$ and $Q=Q(t)$. Previous histological measurements in young children (<10 yr) (Ref. 27) have demonstrated that the cross-sectional shape and area of the ET lumen, in the deformable cartilaginous region, is constant with respect to the long axis of the ET. Since the current study utilizes underdeveloped juvenile monkeys, these measurements are relevant and we, therefore, assume that spatial variations in the ET's area are negligible, i.e., $A=A(t)$ only. Note this assumption may not be valid for fully developed animals since adult ETs exhibit large changes in lumen area and shape.[27] In the following sections we develop and justify the simplified equations used to analyze this model.

Fluid Mechanics

We simplify the description of the fluid mechanics by determining the magnitude of the inertial terms [left-hand side of Eq. (1)] relative to the viscous term using standard dimensional analysis. Consider the ratio of the temporal inertial term to the viscous term,

$$\frac{\rho\partial\mathbf{u}/\partial t}{\mu\nabla^2\mathbf{u}}\sim\frac{\rho\omega U}{\mu U/R^2}=\frac{\rho\omega R^2}{\mu}=\alpha. \tag{3}$$

Here, the velocity is scaled on an average velocity ($\mathbf{u}\sim U$), time is scaled on the frequency of oscillation ($t\sim\omega^{-1}$), the length scale for viscous gradients is the average radius of a fully opened ET ($\nabla^2\sim R^{-2}$), and α is the square of the Wormersly number. The magnitude of α will determine if the temporal inertial term in Eq. (1) can be ignored. We also consider the ratio of the convective inertial term to the viscous term,

$$\frac{\rho(\mathbf{u}\cdot\nabla)\mathbf{u}}{\mu\nabla^2\mathbf{u}}\sim\frac{\rho U^2/L}{\mu U/R^2}=\frac{\rho UR^2}{\mu L}=\frac{\rho Q}{\pi\mu L}=\beta. \tag{4}$$

Here, the length scale for convective gradients is the average length of an ET ($\nabla\sim L^{-1}$), the average velocity is based on the flow rate and the area of a fully opened ET ($U=Q/\pi R^2$), and β is the lubrication Reynolds number. The magnitude of β will determine if the convective inertial term in Eq. (1) can be ignored. For the current experimental conditions of air as the working fluid ($\rho=1.2\text{e}{-3}$ g/cm^3, $\mu=1.8\text{e}{-4}$ g/cm/s), $\omega=2\pi/72$ s (see the Methods section), and an average size ET ($R=0.1$ cm, $L=3$ cm), $\alpha=6\text{e}{-3}$ and $\beta=1\text{e}{-1}$. Since the temporal and convective inertial terms are an order of magnitude smaller than the viscous terms, inertial effects are ignored in this study.

We determine the relationship between flow rate, upstream pressure, and cross-sectional area by solving the simplified version of Eq. (1) (i.e., ignoring inertial terms). The axial velocity field for an arbitrary cross-sectional shape in the xy plane will have the following form:

$$u_z(x,y)=\frac{d_n^2}{\mu L}[p(t)-p_d]F^*(x^*,y^*). \tag{5}$$

Here, d_n is the characteristic length scale for the given cross-sectional shape, $F^*(x^*,y^*)$ is a dimensionless, scale independent, shape factor to be determined, and * indicates dimensionless quantities. Substituting $u_z(x,y)$ into the fully developed, simplified version of Eq. (1) yields the following governing equation and boundary conditions for F^*,

$$\nabla^{*2}F^*=\frac{\partial^2F^*}{\partial x^{*2}}+\frac{\partial^2F^*}{\partial y^{*2}}=-1,$$

$$F^*=0 \quad \text{for } x^*,y^*=S. \tag{6}$$

Here, we have used the characteristic length as a scaling factor, employed the pressure gradient $\{\nabla p=dp/dz=[p(t)-p_d]/L\}$ for fully developed flow $[u_z\neq f(z)]$, and imposed a no-slip boundary condition on the boundary surface S. The shape factor, $F^*(x^*,y^*)$, can be determined once the cross-sectional shape of the ET is specified (see the Appendix).

With an expression for the velocity field, Eq. (5), the time-dependent volumetric flow rate can be expressed as

$$Q(t)=\int_A u_z(x,y)dx\,dy=\frac{d_n^4}{\mu L}[p(t)-p_d]\int_A F^*dx^*dy^*. \tag{7}$$

The time-dependent cross-sectional area is related to the characteristic length by

$$A(t)=\int_A dx\,dy=d_n^2\int_A dx^*dy^*. \tag{8}$$

The pressure drop along the ET can, therefore, be expressed in terms of the cross-sectional area and the flow rate,

$$p(t)-p_d=\frac{\mu L Q(t)}{A(t)^2}\Gamma_S,\quad Q(t)=q_m+q_a\sin[\omega t], \tag{9}$$

where the sinusoidal flow rate, $Q(t)$, is fixed by protocol [$q_m=14$, $q_a=9$, and $\omega=2\pi/(72\text{ s})$]. Γ_S is the hydraulic-geometric shape factor, which is only a function of the cross-sectional shape and is given by $\Gamma_s=(\int_A dx^*dy^*)^2/\int_A F^*dx^*dy^*$. Γ_S is calculated for a variety of elliptical shapes in the Appendix to demonstrate how Γ_S can vary as a function of cross-sectional shape. If convective inertia forces were important, this pressure drop relationship would have to be augmented with a term that is $\sim Q^2$.[2] However, as demonstrated in the parameter estimation section, the current viscous-flow models, which are based on Eq. (9), accurately reproduce the experimental data. This accurate correlation indicates that convective inertial effects are not significant and provides further justification for ignoring these terms. The above analysis also assumes an incompressibility condition, which is validated experimentally in the system verification section.

Structural Mechanics

The mechanical elements supporting the tube wall in Fig. 1, E and μ_w, will be used to describe the ''tube law'' in Eq. (2). Several investigators[4,20,23] have proposed nonlinear functions to describe the tube law of pulmonary airways. These functions are typically singular at $A=0$ since pulmonary airways normally exist in an opened state. The ET, however, is similar to the urethra in that A is identically zero under normal conditions. Therefore, we follow Lecamwasam *et al.*[17] and use a polynomial-type relationship, which is not singular at $A=0$, to describe ET mechanics:

$$\Delta p=p_{\text{mean}}-p_{\text{ext}}=\frac{p(t)+p_d}{2}-p_{\text{ext}}=EA^n(t)+\mu_w\frac{dA(t)}{dt}. \tag{10}$$

Here, p_{ext} is the periluminal pressure that is responsible for keeping the ET in a collapsed configuration, p_{mean} is the mean pressure that exists in the tube, $n\geqslant 1$ allows for higher-order effects, and E and μ_w are the elastic and viscoelastic parameters. Note that E is not the Young's modulus and μ_w is not the dynamic viscosity normally used in the analysis of stress and strain. Although this model assumes no spatial variations in $A(t)$, the pressure must vary between $p(t)$ and p_d. The internal pressure responsible for changes in $A(t)$ is, therefore, defined as the mean pressure, p_{mean}.

Solution Methods

We seek solutions to Eqs. (9) and (10) that can be used to analyze experimental pressure–flow data. We are specifically interested in a data analysis procedure that can estimate ET mechanical properties E, μ_w, and p_{ext}. The solution of Eqs. (9) and (10), however, requires an assumption regarding the downstream pressure, p_d. In this study, we will explore two different assumptions for p_d. First, we set the downstream pressure in the nasopharynx equal to the reference ambient pressure, i.e., $p_d=0$. This assumption is valid for the current experimental conditions in which the animal is anaesthetized with no upper airway obstructions. Under these conditions an analytical solution to Eqs. (9) and (10) is not possible and we, therefore, employ a numerical solution technique. Equation (9) is rewritten in terms of the shape factor, Γ_S, and a shape independent area, $A_2(t)$:

$$A(t)=A_2(t)\Gamma_S^{1/2},\quad \text{where}\quad A_2(t)=\left(\frac{\mu L Q(t)}{p(t)}\right)^{1/2}. \tag{11}$$

A discrete form of $A_2(t)$ can then be calculated from the experimentally measured $p(t)$ and $Q(t)$ assuming that $L=3$ cm for all subjects. Next, a simple three-point central differencing technique[1] can be used to determine the discrete form of $dA_2(t)/dt$. Once $A_2(t)$ and $dA_2(t)/dt$ are known, Eq. (10) can be used to generate a predicted pressure function,

$$\frac{p_{\text{pred}}(t)}{2}=\tilde{E}A_2^n(t)+\tilde{\mu}_w\frac{dA_2(t)}{dt}+p_{\text{ext}}, \tag{12}$$

where $\tilde{E}=E\Gamma_s^{n/2}$ and $\tilde{\mu}_w=\mu_w\Gamma_s^{1/2}$ are shape independent elasticity and wall viscosity parameters. A least-squared regression between $p_{\text{pred}}(t)$ and the experimentally measured $p(t)$ will be performed to determine the free parameters $\tilde{E}$, $\tilde{\mu}_w$, p_{ext}, and n in each animal (see the Parameter Estimation section). Once this regression is performed, $p_{\text{pred}}(t)$ can then be plotted as a function of $Q(t)$ to obtain a visual comparison between the model fit and the experimental data. Since the local pressure–area slope, $dp_{\text{pred}}/dA_2\cong n\tilde{E}A_2^{n-1}$, is a nonconstant function of area, we employ a normalized compliance parameter,

$$\tilde{C}_{\text{norm}} = \left(\frac{\int_{A_{2,\min}}^{A_{2,\max}} n\tilde{E} A_2^{n-1} dA_2}{A_{2,\max} - A_{2,\min}} \right)^{-1}, \qquad (13)$$

to describe the global compliance of the ET. Here, $A_{2,\max}$ and $A_{2,\min}$ are the maximum and minimum shape independent areas calculated from Eq. (11). Note that this analysis does not require *a priori* knowledge of the ET's cross-sectional shape (i.e., knowledge of Γ_S).

In the second approach, we seek a simplified model that can be solved analytically and, therefore, assume $p_d = p_{\text{ext}}$ and a linear tube law ($n=1$). Note that these assumptions are primarily employed to obtain an analytical solution and may not have any direct physiological significance. With these conditions, Eqs. (9) and (10) can be solved analytically to yield a function relating cross-sectional area to time,

$$A(t) = \Gamma_s^{1/2} A_2(t) = \Gamma_s^{1/2} \left(\frac{\mu L (9\tilde{E}^2 q_m + \omega^2 q_m \tilde{\mu}_w^2 - 3\tilde{E}\omega q_a \tilde{\mu}_w \cos[\omega t] + 9\tilde{E}^2 q_a \sin[\omega t])}{18\tilde{E}^3 + 2\tilde{E}\omega^2 \tilde{\mu}_w^2} \right)^{1/3}. \qquad (14)$$

With this expression for $A(t)$ [and the specified $Q(t)$], Eq. (9) can be used to generate a predicted pressure, $p_{\text{pred}}(t)$, which will be a function of three free parameters ($\tilde{E}$, $\tilde{\mu}_w$, and p_{ext}). This analytical predicted pressure will be plotted as a function of the flow rate, $Q(t)$, to determine how each parameter affects the pressure-flow rate relationship. In addition, alternative parameter values will be determined for each animal by performing a similar least-squared analysis between this analytical $p_{\text{pred}}(t)$ and $p(t)$. Note that for this linear tube-law model, the normalized compliance is simply $\tilde{C}_{\text{norm}} = 1/\tilde{E}$. As a result, we will be able to evaluate the affect of the downstream pressure and linear tube-law assumptions by comparing parameter values from the numerical ($p_d = 0$) and analytical ($p_d = p_{\text{exp}}, n=1$) models. *As demonstrated in the Results section, the choice of model does not substantially affect the magnitudes of compliance and wall viscosity obtained when these models are correlated with experimental data.*

METHODS AND MATERIALS

The instrumentation used in the forced-response test is shown in Fig. 2. Two 60 cc plastic syringes are used to generate airflow via a computer-controlled syringe pump (Harvard Apparatus, Pump-22). The airflow rate is measured with a mass flow sensor (Honeywell, model PK 8854 0) and the pressure is monitored with a standard pressure transducer (Honeywell, model PK 8780 2). The mass flow rate is converted to a volumetric flow rate assuming constant density. The HP VEE data acquisition routine (Agilent Technologies) is used to record the flow rate and pressure as a function of time and to control the syringe pump. A 22g sterile needle is used to create a ~1 mm slit-like opening in the TM for access to the ME. An airtight seal is then formed between the test system and the external ear canal. The pressure loss in the system tubing at the maximum flow rate ($Q = 23$ cc/min) was measured at < 2 mm H_2O. In addition, the nonrecoverable pressure loss across the TM was calculated at < 1 mm H_2O for a 1-mm-diam orifice in a 3-mm-diam TM at maximum flow.[34] Therefore, the ME pressure will be identical to the pressure measured at the syringe.

For this study, data were obtained from 12 cynomolgus monkeys (*Macaca fascicularis*, 2–4 kg) with freshly created myringotomy perforations and otherwise normal ME status as described by Ghadiali *et al.*[12] This animal model was chosen since previous investigators[7] have

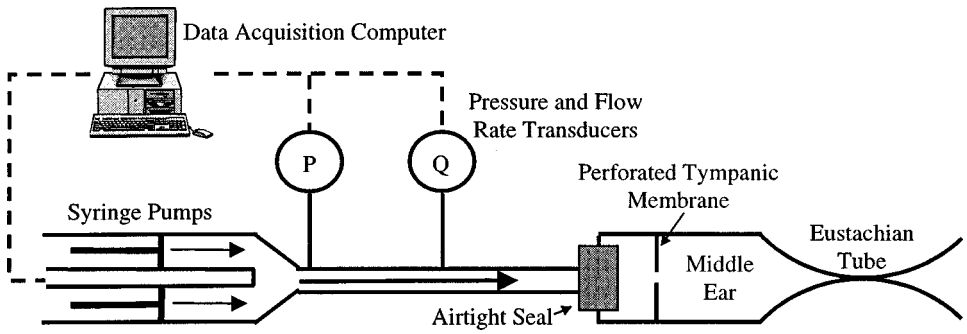

FIGURE 2. Schematic of force-response instrumentation used to control and measure air flow rate and pressure in the ET.

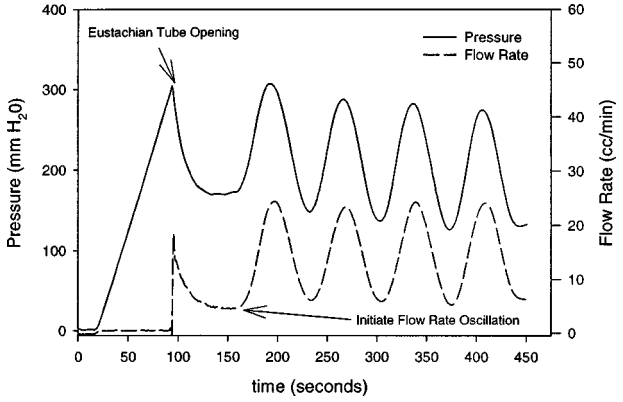

FIGURE 3. Typical pressure and flow rate measurements made as a function of time during a modified forced-response test.

demonstrated a correlation between ET function in monkeys and humans. For each session, the animals were sedated with 30 mg ketamine and then anesthetized with ''monkey mix'' (10 mg/kg ketamine, 2 mg/kg xylazine, and 0.3 mg/kg acepromazine). This level of anesthesia immobilized the animal's swallowing reflex. Once standard force-response test measurements, including the TCI, were obtained in the left ear, the modified compliance test was implemented as discussed below. All protocols used in this study were approved by the Children's Hospital of Pittsburgh Animal Research and Care Committee.

During a standard forced-response test, the ME is inflated at a constant flow rate via the syringe pump until the ET opens. Once opened, the pump continues to deliver a steady flow through a partially open ET until steady-state pressure and flow rates are obtained. This standard test was conducted using flow rates of 5.6, 11.5, and 23 cc/min. Resistance at each flow rate was calculated as the ratio of steady-state pressure to steady-state flow, and the TCI was calculated as the ratio of resistances at 5.6 and 23 cc/min.[29] In the modified force-response test (Fig. 3), the ME is inflated in a similar manner. However, once the ET is open, the syringe pump is programed to impose a sinusoidal flow rate between 5.0 and 23 cc/min with a period of 72 s, and the pressure and flow rate are measured simultaneously until a pseudo-steady-state, defined as a $<5\%$ change in the maximum and minimum pressure between two successive oscillations, is obtained (Fig. 3). The pressure and flow rate during this pseudo-steady-state cycle is used for data analysis. This modified force response protocol was performed three times in each subject to determine the reproducibility of the results. An analysis of these repeated measurements with the numerical model indicate that the standard error for the compliance parameter was $<7\%$ while the standard error for the wall viscosity parameter was $<15\%$. Since it is not practical to conduct these types of tests for longer than $\sim$5–10 min in young children with ear disease, this protocol was limited to a single maneuver (i.e., a single frequency and flow rate magnitude).

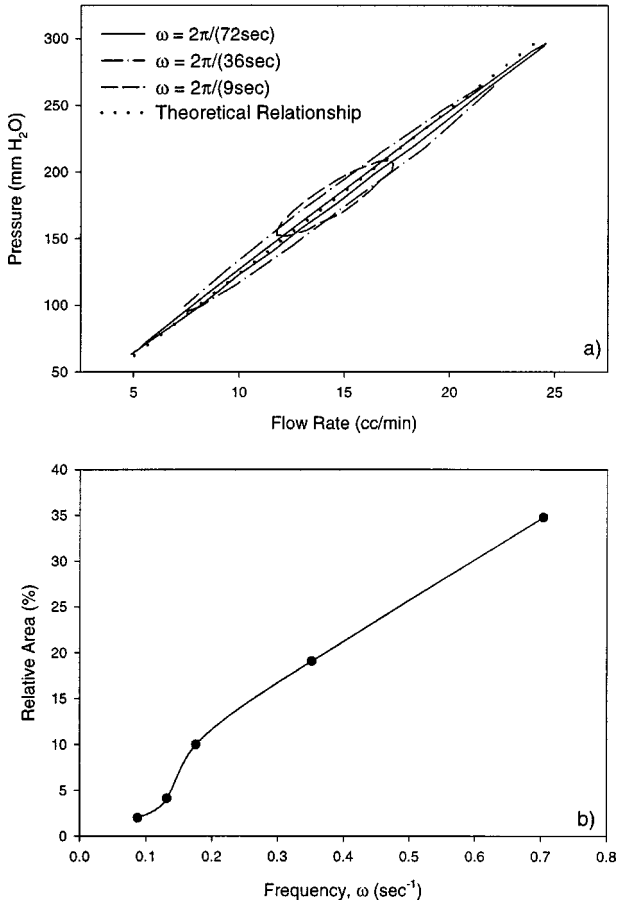

FIGURE 4. Verification of incompressible fluid behavior. (a) Pressure vs. flow rate relationships for a rigid tube as function of frequency. (b) Relative area as a function of frequency for a rigid tube. Relative area <2% at lowest frequency indicates minimal hysteresis and incompressible fluid behavior.

System Verification

The fluid mechanic model presented above assumes the incompressible, viscous driven flow of air in the ET under experimental conditions. We have performed the following system verification test to determine if these conditions are satisfied. The instrumentation shown in Fig. 2 was attached to a rigid metal tubing (0.3 mm diam, 8.0 cm length). Since the amount of gas compression will depend on the magnitude of the mean pressure in the system, the dimensions of this rigid tubing were chosen such that the mean pressure at $Q=14$ cc/min ($p\sim200$ mm H_2O) is the same magnitude as the mean pressure observed in the animal experiments (see Fig. 3).

Several tests were conducted on this rigid tubing by programing the syringe pump to produce flow rate oscillations, $Q(t)=14+9\sin(\omega t)$ cc/min, at various frequencies (ω). The measured pressure–flow rate relationship for a single cycle in the rigid tube at three different frequencies is shown in Fig. 4(a). Under these conditions, an incompressible, viscous driven flow would produce a linear relationship between the pressure and flow [dotted line in Fig. 4(a)] with no difference in the inflation and deflation phases (i.e., no hysteresis). The degree of hysteresis at different frequencies can be compared by calculating the relative hysteresis loop area,

$$\text{Relative Area}=\frac{\text{Hysteresis Loop Area}}{(p_{\max}-p_{\min})(Q_{\max}-Q_{\min})}*100\%. \tag{15}$$

Here, the hysteresis loop area was calculated by integration, $p_{\max}$ is the maximum recorded pressure, $p_{\min}$ is the minimum pressure, $Q_{\max}$ is the maximum flow rate, and $Q_{\min}$ is the minimum flow rate. As demonstrated in Fig. 4(b), significant hysteresis exists at high frequencies while at low frequencies the hysteresis is substantially reduced. The reduction in loop area as a function of frequency, shown in Fig. 4(b), indicates that air behaves like an incompressible fluid at low frequencies. The current experimental protocol, therefore, uses the lowest feasible frequency, $\omega=2\pi/(72\text{ s})$.

RESULTS

Simulation Results

We have performed two separate parameter variation studies to understand how the magnitude of the mechanical properties of the ET, namely, compliance ($\tilde{C}_{\text{norm}}=1/\tilde{E}$) and wall viscosity ($\tilde{\mu}_w$), can independently effect the pressure–flow rate relationship. For a given set of parameter values, Eq. (14) is used to calculate the variation in the shape independent area, $A_2(t)$. Since $Q(t)$ is a known sinusoidal function, Eqs. (9) and (14) can be used to calculate the pressure as a function of time, $p(t)$, given a collapsible length, $L=3$ cm; linear tube law, $n=1$; the viscosity of air; and a downstream pressure, $p_d=p_{\text{ext}}=0$. As a result, the pressure–flow rate relationship can be investigated for a variety of parameter values by plotting $p(t)$ as a function of $Q(t)$. The set of base parameters used in both simulations are, $q_m=14$ cc/min, $q_a=9$ cc/min, $\omega=2\pi/(72\text{ s})$, $p_{\text{ext}}=0$ mm H_2O, $\tilde{C}_{\text{norm}}=5\text{e}{-7}$ cm^2/mm H_2O, and $\tilde{\mu}_w=1.25\text{e}9$ poise/cm^2. Although we are using Eq. (14) of the analytical model ($p_d=p_{\text{ext}}$), the $p_{\text{ext}}=0$ condition insures that the results of this simulation will be identical to using the $p_d=0$ numerical model.

First, the influence of tubal compliance is investigated by constructing pressure–flow relationships using the base parameters and various compliance values, as shown in Fig. 5(a). For a given flow rate, the resulting pressures are larger in the rigid (lower compliance) tube than the pressures observed in a flexible (higher compliance) tube. From Eq. (9), higher pressures at a given flow rate would indicate a smaller opening area at low compliance values, which is verified in Fig. 5(b). Conversely, at a higher compliance value, the opening area is larger such that there is less resistance to flow and thus the pressures are lower. The average slope of the pressure–flow rate hysteresis loop, dp/dQ, in compliant tubes is smaller than the slope observed in the more rigid tubes. This phenomenon is directly related to the pressure–area relationships shown in Fig. 5(b), which are constructed by plotting $p(t)$ as a function of $A_2(t)$. At high compliance values the slope of the p vs. A_2 curve is small as would be expected based on the definition of compliance, $\tilde{C}=dA_2/dp$. As a result, the pressure magnitude does not vary significantly as a function of area. These small changes in pressure during the oscillation cycle translate into small changes in pressure as a function of flow rate and thus a small dp/dQ at high compliance values [Fig. 5(a)]. Conversely, at low compliance values, the p vs A_2 slope is much larger [Fig. 5(b)] such that the pressure magnitude varies considerably as a function of area. As a result, these larger changes in pressure result in a larger dp/dQ at low compliance values.

The influence of wall viscosity is investigated by constructing pressure–flow relationships using the base parameter values and various wall viscosity values, as shown in Fig. 5(c). For low wall viscosity values, the tube wall is essentially modeled as a linear-elastic material, i.e., Eq. (10) with $\tilde{\mu}_w=0$. Under these conditions the material behaves similarly on inflation and deflation and thus the hysteresis loop area is minimal. However, as $\tilde{\mu}_w$ increases, the viscoelastic element induces a time delay which results in a difference between the inflation and deflation phase and thus an increase in the hysteresis loop area. The hysteresis loop direction is governed by the time-dependent functions, $p(t)$ and $Q(t)$, and is indicated by arrows in Figs. 5(c) and 5(d). This clockwise direction can be elucidated by considering two time points labeled A and B, which have the same flow rate but are on the inflation (A) and deflation (B) phases. During inflation the viscous element delays the opening of the tube while on deflation the viscous element delays the collapse of the tube. Therefore, at a given flow rate, the opening area during inflation [point A, Fig. 5(d)] will be slightly less than the opening area during deflation (point B). As a result, the pressure on inflation is larger than the pressures on deflation. These simulation results

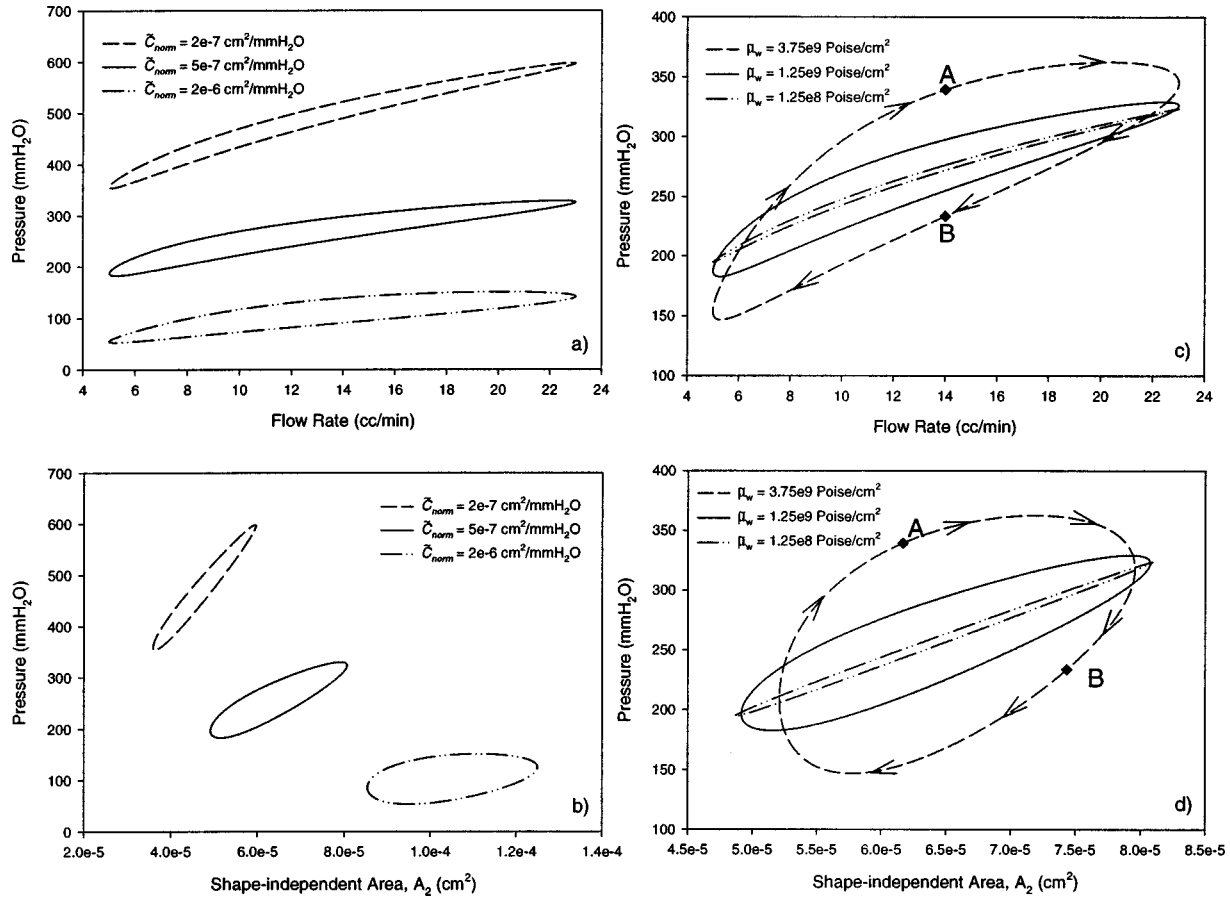

FIGURE 5. Simulation of pressure vs. flow rate and pressure vs. area hysteresis loops using the $p_d = p_{ext}$ analytic model. The normalized compliance parameter, $\tilde{C}_{norm}$, effects the slope of both the (a) pressure–flow rate and the (b) pressure–area hysteresis loops. The wall viscosity parameter, $\tilde{\mu}_w$, effects the area of both the (c) pressure–flow rate and the (d) pressure–area hysteresis loops.

indicate that the shape of the pressure–flow rate hysteresis loop will be a function of the compliance and wall viscosity parameters. In the remainder of this paper we will use these models to analyze the experimental data.

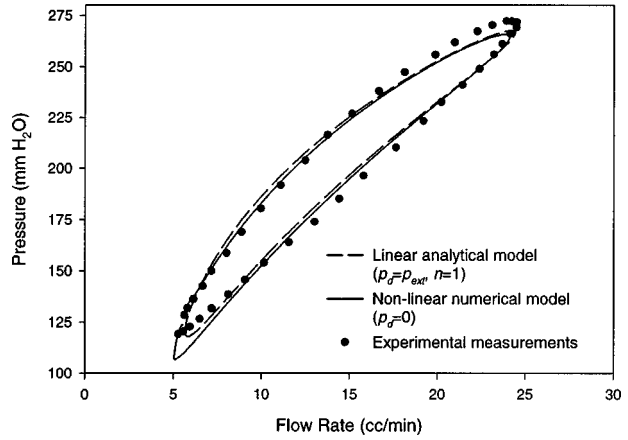

FIGURE 6. Correlation of experimental and theoretical pressure–flow rate hysteresis loops using the viscoelastic analytical and numerical models.

Parameter Estimation

The experimental pressure and flow rate measurements shown in Fig. 3 can be used to generate a pressure–flow rate hysteresis loop by plotting the pressure, $p(t)$, as a function of the flow rate, $Q(t)$, during one cycle recorded at convergence (solid points in Fig. 6). These pressure/flow data can be correlated with both the numerical and analytical models to determine estimates of ET mechanical properties. First, we investigate the ability of the numerical ($p_d = 0$) model to capture the experimental pressure/flow data. A least-squared analysis is performed by using a nonlinear regression technique [IMSL routine DRLIN (Ref. 33)] to vary the free parameters ($\tilde{E}$, $\tilde{\mu}_w$, p_{ext}, and n) and to obtain the best fit between the numeric $p_{pred}(t)$ function and the experimentally measured $p(t)$. The ability of this regression technique to simulate the experimental behavior is shown by the solid line in Fig. 6, in which $p_{pred}(t)$ is plotted as a function of $Q(t)$. This complete viscoelastic model

TABLE 1. Comparison of the normalized shape independent compliance, shape independent wall viscosity, and periluminal pressure obtained in each animal using the linear analytical ($p_d = p_{ext}, n=1$) and nonlinear numerical ($p_d = 0$) models. Nonlinear parameter n obtained using the numerical model is also presented.

Monkey No.	$\tilde{c}^{ana}_{norm}$ ($\times 10^{-7}$ cm^2/mm H$_2$O)	$\tilde{c}^{num}_{norm}$ ($\times 10^{-7}$ cm^2/mm H$_2$O)	$\tilde{\mu}^{ana}_w$ ($\times 10^8$ poise/cm^2)	$\tilde{\mu}^{num}_w$ ($\times 10^8$ poise/cm^2)	p^{ana}_{ext} (mm H$_2$O)	p^{num}_{ext} (mm H$_2$O)	n
1	5.77	5.84	9.60	13.14	−60	0	1.57
2	1.86	1.65	11.65	21.18	−209	19	2.89
3	2.33	2.30	1.44	1.57	−130	86	3.80
4	3.92	3.93	5.78	6.91	−36	43	1.78
5	1.34	1.34	5.31	0	−377	0	3.77
6	4.23	4.07	8.11	12.38	−103	17	1.73
7	5.33	5.53	6.48	9.58	−109	40	3.99
8	5.45	5.59	8.47	10.60	−58	23	1.96
9	5.00	4.14	2.50	5.11	−120	0	2.99
10	4.54	4.55	6.77	8.91	−68	16	1.83
11	1.55	1.16	0.05	0.56	−288	9	3.66
12	3.25	3.15	9.36	13.55	−109	3	1.88
Average ± std.	3.71 ± 1.61	3.61 ± 1.68	6.29 ± 3.51	8.62 ± 6.22	−139 ± 102	21 ± 25	2.65 ± 0.96

accurately captures both the curvature and hysteresis of the measured pressure–flow rate data, thus indicating that both wall elastance and viscosity should be included in the description of ET mechanics. For each animal's ET, the best-fit parameter values from this numerical model were used to estimate the normalized compliance parameter, $\tilde{C}^{num}_{norm}$, from Eq. (13); the wall viscosity parameter, $\tilde{\mu}^{num}_w$; the periluminal pressure, p^{num}_{ext}; and the coefficient, n. Table 1 list the average values of $\tilde{C}^{num}_{norm}$, $\tilde{\mu}^{num}_w$, p^{num}_{ext}, and n obtained from three repeated measurements in each animal as well as the average and standard deviations for each parameter.

The ability of the regression technique to uniquely determine ET mechanical properties was investigated by calculating a coefficient of variation (CV) for each parameter. Specifically, for each regression the IMSL routine DCOVB (Ref. 33) was used to calculate the asymptotic estimated variance–covariance matrix, V. The standard error of the ith parameter, calculated as the square root of the ith diagonal of V, was normalized to determine each parameter's CV. The CV values for all parameters were consistently $<10\%$ except for $\tilde{\mu}^{num}_w$ in animal 5 where $\tilde{\mu}^{num}_w \sim 0$. Thus, the current regression technique uniquely determines ET mechanical properties from the measured pressure and flow rate data.

The measured pressure–flow rate functions were also analyzed with the analytical ($p_d = p_{ext}$) model to investigate the influence of the downstream pressure condition. As above, a regression analysis was performed by varying the free parameters ($\tilde{E}$, $\tilde{\mu}_w$, p_{ext}) to obtain the best fit between the analytical $p_{pred}(t)$ and $p(t)$. As shown by the dashed line in Fig. 6, this analytical model also accurately simulates the experimental data. The best-fit parameter values from this analytical model were used as alternative estimates of compliance $\tilde{C}^{ana}_{norm} = 1/\tilde{E}$, wall viscosity, $\tilde{\mu}^{ana}_w$, and periluminal pressure, p^{ana}_{ext}. The mean values of these parameters from three repeated measurements are presented in Table 1 along side the "numerical" model results (negative p^{ana}_{ext} values are explained in the Discussion section). Linear regressions between "numerical" and "analytical" results indicate that $\tilde{C}^{num}_{norm} = 0.98(\tilde{C}^{ana}_{norm})$, $r^2 = 0.97$ while $\mu^{num}_w = 1.4(\mu^{ana}_w)$, $r^2 = 0.80$. Therefore, the numerical and analytical estimates of compliance are nearly identical while the estimates of wall viscosity are strongly correlated but generally lower in the analytical model.

DISCUSSION

We have developed a modification of the standard forced-response test that yields continuous pressure–flow rate data. A simple fluid-structure model of airflow in a collapsed tube was developed and correlated with experimental pressure–flow rate hysteresis loops. This technique was used to estimate several mechanical properties, including ET compliance, $\tilde{C}_{norm}$, and wall viscosity, $\tilde{\mu}_w$, in 12 cynomologus monkeys. The goal of the current testing technique and mathematical models was to provide a method that can accurately determine ET mechanical properties and to provide an alternative to current testing methods, which may not be clinically practical or highly accurate.

The tubal compliance index, which is the ratio of resistance (pressure/flow) at two separate flow rates, is currently the most commonly reported measure of ET mechanics.[21,22,24,25,29,30] Since the TCI is based on variations in resistance, it may contain information regarding distensability, but it is only a summary measure that does not conform with the engineering definition of compliance ($dA/d\Delta p$). The TCI was calculated in each animal

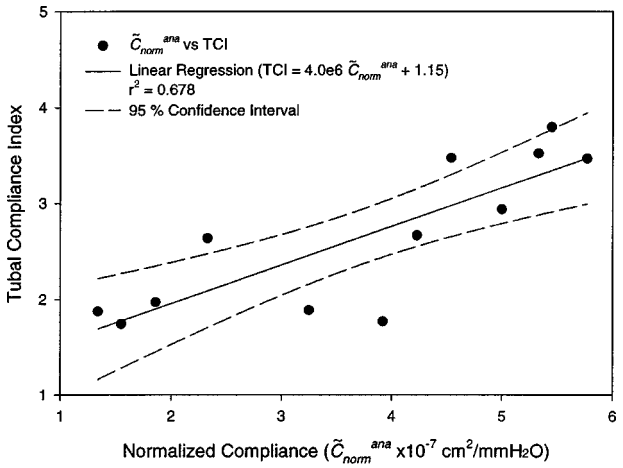

FIGURE 7. Relationship between the tubal compliance index (TCI) and the normalized compliance parameters obtained from the analytical model, $\tilde{C}_{\text{norm}}^{\text{ana}}$.

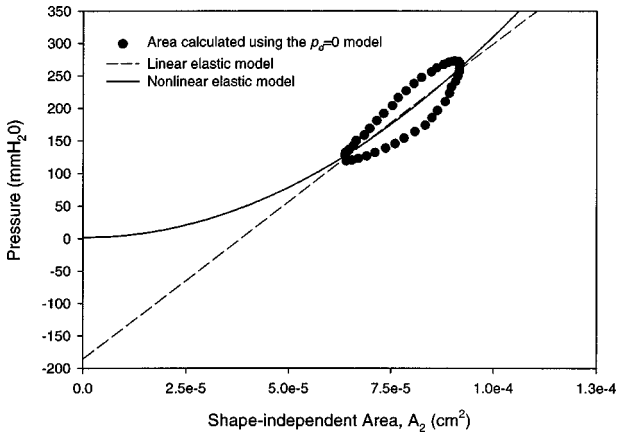

FIGURE 8. Pressure vs. area relationship demonstrating the breakdown of the linear model near the $A_2=0$ intercept. Area is calculated using the numerical model equations.

and plotted as a function of the current measure of compliance obtained from the analytical model, $\tilde{C}_{\text{norm}}^{\text{ana}}$ (Fig. 7) to investigate the relationship between these two measures. Although these measures appear to be linearly related, (TCI$=4.0\text{e}6\tilde{C}_{\text{norm}}^{\text{ana}}+1.15$), the correlation coefficient, which is a measure of the shared variance, of this relationship is only 68%. The TCI may, therefore, not be an accurate measure of compliance and cannot be used as a parametric estimator in formal descriptions of ET mechanics. In contrast, the current estimate of compliance, $\tilde{C}_{\text{norm}}^{\text{ana}}$, is based on the engineering definition and is, therefore, a more accurate measure of how much pressure must be applied to increase the ET lumen cross-sectional area. In addition, the current testing technique has the advantage of being able to determine time-dependent mechanical properties (i.e., wall viscosity).

Although previous ET studies have not measured the engineering compliance, other investigators have measured $dA/d\Delta p$ in other collapsible biological tubes.[9,17] To compare the current results with those measurements, the shape independent compliance parameter, $\tilde{C}_{\text{norm}}^{\text{ana}}$, must be converted into the shape dependent parameter, $dA/d\Delta p$. Specifically, Eq. (10) with $\mu_w=0$ and the definition $\tilde{C}_{\text{norm}}^{\text{ana}}=1/\tilde{E}=1/(E\Gamma_s^{1/2})$ can be used to calculate $dA/d\Delta p=\tilde{C}_{\text{norm}}^{\text{ana}}\Gamma_s^{1/2}$. Previous histological measurements[27] indicate that the shape of the ET lumen is elliptical with a length-to-width ratio ~7:1. This shape can be used to calculate $\Gamma_s=90$ (see the Appendix), and thus the average $\tilde{C}_{\text{norm}}^{\text{ana}}$ value presented in Table 1 can be used to calculate $dA/d\Delta p=5\text{e}-5$ cm^2/mm Hg. This value is comparable to the magnitude obtained in the brachial artery[9] (10e−5 cm^2/mm Hg), and an order of magnitude lower than the maximum compliance obtained in the urethra[17] (5e−4 cm^2/mm Hg). The current analysis, therefore, predicts reasonable compliance values and suggests that the ET is more rigid than other collapsible biological tubes.

In this study, we have analyzed experimental data with two separate mathematical models. As demonstrated in Table 1, the linear analytical model, which uses a linear tube law, predicts $p_{\text{ext}}<0$ while the numerical model, with a nonlinear tube law, predicts $p_{\text{ext}}>0$. Negative external pressures are not consistent with the physiological conditions of a collapsed ET under normal conditions. To better understand why the linear analytical model predicts a negative p_{ext} value, consider the pressure versus area data shown in Fig. 8. Here, the shape independent area is calculated using Eq. (11) and the measured pressure and flow rate data shown in Fig. 6. When these data are correlated with the linear–elastic solid model [Eq. (12), $\tilde{\mu}_w=0$, $n=1$], the $A_2=0$ intercept predicts that $p_{\text{ext}}<0$ (see the dashed line in Fig. 8). This negative intercept, however, may not represent the true external pressure since it is likely that the pressure vs. area relationship is highly nonlinear. The pressure–area data can also be correlated with the nonlinear numerical model ($n\neq 1, \tilde{\mu}_w=0$), as shown by the solid line in Fig. 8. Although this nonlinear model results in a similar relationship in the region of experimental measurements, it predicts a positive intercept ($p_{\text{ext}}>0$). These results suggest that accurate descriptions of ET mechanics may require a nonlinear tube law. However, Table 1 also demonstrates that both models yield similar results for the normalized compliance and wall viscosity parameters. Therefore, although the inconsistent $p_{\text{ext}}<0$ results obtained in the linear analytical model can be accounted for with a nonlinear numerical model, a relatively accurate determination of compliance and wall viscosity can be obtained from either model.

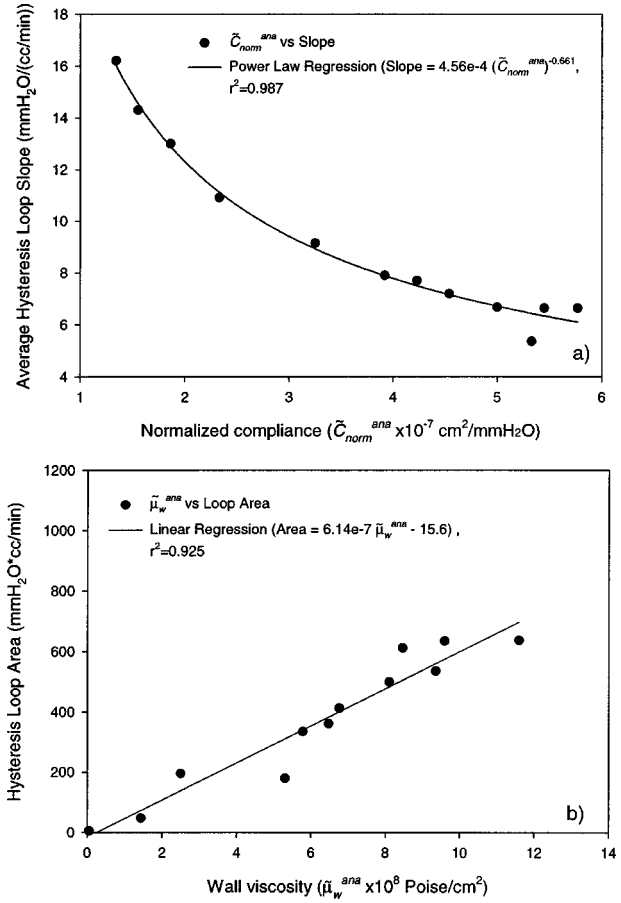

FIGURE 9. Comparison of (a) average hysteresis loop slope and the predicted compliance values and (b) hysteresis loop area and the predicted tube wall viscosity values.

To be a useful diagnostic tool the testing method and the mathematical models used to extract the mechanical properties must be easy to implement in a clinical setting. The current testing procedure is based on the minimally invasive standard force-response test that has been used previously by clinical investigators.[6] The main modification we have developed in this study is the application of an oscillatory flow rate once the ET is opened. Since this modification is minor in terms of implementation, the current testing procedure can be readily used in a clinical setting. The determination of ET mechanical properties can be performed using both a numerical model with standard downstream pressure boundary conditions and an alternative analytical model which analyzes experimental data with a relatively simple closed-form solution, Eq. (14). The analytical technique would be relatively easy to implement in a clinical setting. By contrast the numerical model requires a more complicated analysis based on a finite-differencing technique and, therefore, may not be practical in a clinical environment. We have, however, demonstrated that the estimates of compliance and wall viscosity obtained from the analytical model do not differ significantly from the estimates obtained from the numerical model, and thus the use of the analytic model in a clinical setting is justified.

If the computational resources are not available to perform the least-squared analysis, it may also be possible to use the slope and area of the pressure–flow hysteresis loop as preliminary estimates of compliance and wall viscosity. We investigate the relationship between loop properties and the mechanical parameters by plotting the slope and area as a function of $\tilde{C}_{\text{norm}}^{\text{ana}}$ and $\tilde{\mu}_w^{\text{ana}}$ for all animals in Fig. 9. Here, analytic model results are used since this model is more likely to be used by clinicians. The nonlinear relationship between the average slope and $\tilde{C}_{\text{norm}}^{\text{ana}}$ shown in Fig. 9(a) can accurately be correlated with a power-law relationship (slope $=4.56\text{e}{-4}(\tilde{C}_{\text{norm}}^{\text{ana}})^{-0.661}$, $r^2=0.987$). This relationship can be understood by considering a solution to Eqs. (9), (10), and (11) with $p_d=p_{\text{ext}}$, $n=1$, and $\tilde{\mu}_w=0$:

$$A_2^3(t)=\frac{\mu L Q(t)}{2\tilde{E}}. \tag{16}$$

From this relationship we can estimate $dA_2/dQ\sim\tilde{C}_{\text{norm}}^{1/3}$ using the definition $\tilde{C}_{\text{norm}}=1/\tilde{E}$. Since $dp/dA\sim\tilde{C}_{\text{norm}}^{-1}$ [Eq. (10)], the slope $(dp/dQ=dp/dA\,dA/dQ)$ will be proportional to $\tilde{C}_{\text{norm}}^{-2/3}$ as predicted by the nonlinear relationship shown in Fig. 9(a). Figure 9(b) demonstrates that the hysteresis loop area and $\tilde{\mu}_w^{\text{ana}}$ can be correlated with a linear relationship (area$=6.14\text{e}{-7}\tilde{\mu}_w^{\text{ana}}-15.6$, $r^2=0.925$). Thus, the average slope of the pressure–flow hysteresis loop could be used as an indicator of compliance, while the hysteresis loop area could be used as an indicator of wall viscosity.

Limitations and Future Studies

As with any model study, the current mathematical models, which are able to quantify ET mechanical properties, do contain potential limitations. First, the ET's pressure–area relationship (tube law) is assumed to be a simple polynomial relationship in the numerical model. Several investigators have, however, measured more complex nonlinear pressure–area relationships for other biological tubes.[3,10,31] Future studies will, therefore, employ magnetic resonance imaging (MRI) techniques[28] to obtain a direct measurement of the ET's pressure–area relationship. The MRI scans will be used to measure the cross-sectional area while concurrent pressure measurements will be made via the force-response system. We will, therefore, be able to examine the conditions under which this polynomial pressure–area relationship is valid. These MRI-based experiments will also provide an

alternative and more direct method of calculating the compliance ($dA/d\Delta p$) of the ET. If a positive correlation exists, the current technique, which is significantly less expensive, may provide clinicians with a valuable method for determining ET mechanical properties.

The current models also assume that the longitudinal tension is sufficient to prevent spatial variations in cross-sectional area. Although this assumption is supported by *ex vivo* histological measurements in young children,[27] this assumption may not be valid in adults due to large changes in lumen area and shape. Future studies will, therefore, use MRI techniques to determine the extent and importance of these *in vivo* spatial variations and will also include a more-detailed finite-element-based analysis of the equations that govern the complex fluid-structure interactions.

In summary, we have developed an engineering technique to determine the mechanical properties of the ET. Compliance and wall viscosity parameters were determined by correlating both numeric and analytic mathematical models of airflow in the ET with experimental pressure–flow rate data. This technique is significantly more sophisticated than current clinical testing techniques in that the compliance of the tube is based on engineering principles and the viscoelastic nature can be quantified. In addition, both the numeric and analytic models yield similar estimates of compliance and wall viscosity. The analytic model, which is the most clinically applicable model, will, therefore, be used in future studies to explore the physical contributors to ET mechanics. For example, the size and composition of the ET cartilage, the surface condition of the mucosa lining layer, and the resting tonus of the musculature are all expected to affect ET mechanics. Future studies will therefore include the measurement of mechanical properties before and after paralysis of the tensor veli palatini muscle and installment of surface active agents to the mucosa (surfactant replacement therapy). As a result, we will be able to determine if a particular factor is an important determinant of ET mechanics. Identification of these factors may lead to more effective treatment strategies for patients with chronic OM.

APPENDIX: CALCULATION OF THE HYDRAULIC–GEOMETRIC SHAPE FACTOR

The first step in calculating the hydraulic–geometric shape factor, $\Gamma_s = (\int_A dx^* dy^*)^2 / \int_A F^* dx^* dy^*$, is to determine the shape factor function, $F^*(x^*, y^*)$ from Eq. (6) for a given cross-sectional shape. Since the cross-sectional shape of the ET could be quite complex, we have used the FlexPDE© general purpose finite-element software system (PDE Solutions Inc, Antioch, CA) to obtain numerical solutions to the partial differential equation. For this set of calculations, the problem domain consisted of elliptical cross sections with various length-to-width ratios. Once the domain is specified, Eq. (6) is used as the field equation and the appropriate Neuman boundary condition ($F^* = 0$) is applied to the boundary. The FlexPDE© software's automatic mesh generation and adaptive mesh refinement capabilities are used during the solution process. Once a solution for F^* is obtained, the appropriate integrals are also calculated by the software package. Figure 10 demonstrates how Γ_s can vary for different geometric shapes and that for a given cross-sectional area the resistance to flow is minimized by a circular cross section. In addition, the calculated value of Γ_s for a circular cross section (25.136) is in excellent agreement with the theoretical value ($8\pi = 25.133$), thus validating the computational approach. Since this technique can be used for any arbitrary cross-sectional geometry, it is particularly suited to biological systems such as the ET where the geometry is complex.

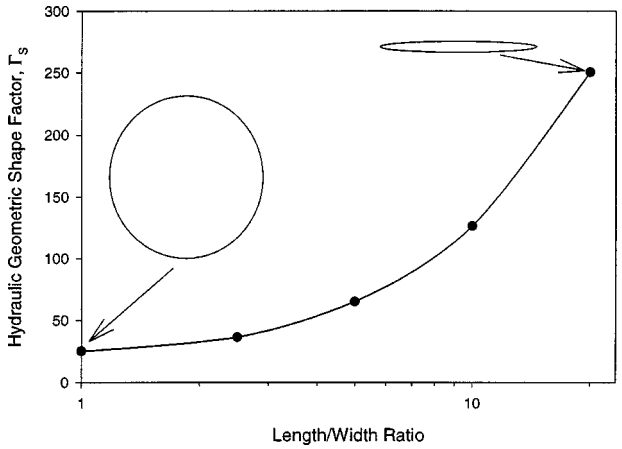

FIGURE 10. Variation of the hydraulic–geometric shape factor for various length-to-width ratio elliptical cross sections. This figure indicates that for a given cross-sectional area, the resistance to flow is minimal for a circular cross section.

ACKNOWLEDGMENTS

The authors thank Julie Banks for her invaluable assistance in conducting the animal experiments, Dr. William Karanavas for his assistance in developing and maintaining the forced-response system, and Dr. Laura Lund for her assistance with the sensitivity analysis. This research was supported in whole or in part by the Children's Hospital of Pittsburgh and National Institute for Deafness and other Communication Disorders Grant No. P01 DC01260.

REFERENCES

[1] Anderson, J. D. Basic aspects of discretization. In: Computational Fluid Dynamics: The Basics with Applications, ed-

ited by J. J. Corrigan and E. Castellano. New York: McGraw-Hill, 1995, pp. 125–167.
[2] Barnea, O., and G. Gillon. Model-based estimation of male urethral resistance and elasticity using pressure-flow data. *Comput. Biol. Med.* 31:27–40, 2001.
[3] Bassez, S., P. Flaud, and M. Chauveau. Modeling of the deformation of flexible tubes using a single law: Application to veins of the lower limb in man. *J. Biomech. Eng.* 123:58–65, 2001.
[4] Bertram, C. D., C. J. Raymond, and K. S. Butcher. Oscillations in a collapsed-tube analog of the brachial artery under a sphygmomanometer cuff. *J. Biomech. Eng.* 111:185–191, 1989.
[5] Bluestone, C. D., and J. O. Klein. Physiology, pathophysiology, and pathogenesis. In: Otitis Media in Infants and Children, edited by S. S. Donley. Philadelphia: Saunders, 2001.
[6] Bluestone, C. D., S. E. Stool, and M. A. Kenna. Otitis media, atelectasis, and eustachian tube dysfunction. In: Pediatric Otolaryngology, edited by C. D. Bluestone and J. O. Klein. Philadelphia: Saunders, 1996, pp. 388–582.
[7] Cantekin, E. I., W. J. Doyle, and C. D. Bluestone. Comparison of normal eustachian tube function in the rhesus monkey and man. *Ann. Otol. Rhinol. Laryngol.* 91:179–184, 1982.
[8] Cantekin, E. I., C. A. Saez, C. D. Bluestone, and S. A. Bern. Airflow through the eustachian tube. *Ann. Otol. Rhinol. Laryngol.* 88:603–612, 1979.
[9] Drzewiecki, G., and J. J. Pilla. Noninvasive measurement of the human brachial artery pressure–area relation in collapse and hypertension. *Ann. Biomed. Eng.* 26:965–974, 1998.
[10] Elad, D., M. Sahar, J. M. Avidor, and S. Einav. Steady flow through collapsible tubes—Measurements of flow and geometry. *J. Biomech. Eng.* 114:84–91, 1992.
[11] Gaver, D. P., D. Halpern, O. E. Jensen, and J. B. Grotberg. The steady motion of a semi-infinite bubble through a flexible-walled channel. *J. Fluid Mech.* 319:25–65, 1996.
[12] Ghadiali, S., W. J. Federspiel, J. D. Swarts, and W. J. Doyle. Measurement of the viscoelastic compliance of the eustachian tube using a modified force-response test. *Auris Nasus Larynx* 29:1–5, 2002.
[13] Heil, M. Airway closure: Occluding liquid bridges in strongly buckled elastic tubes. *J. Biomech. Eng.* 121:487–493, 1999.
[14] Heil, M. Stokes flow in an elastic tube—A large-displacement fluid-structure interaction problem. *Int. J. Numer. Methods Fluids* 28:243–265, 1998.
[15] Kaneko, A., T. Doi, Y. Hosoda, T. Iwano, and T. Yamashita. Direct measurement of eustachian tube compliance. *Acta Oto-Laryngol.* 116:594–598, 1996.
[16] Kaneko, A., Y. Hosoda, T. Doi, N. Tada, T. Iwano, and T. Yamashita. Tubal compliance—Changes with age and in tubal malfunction. *Auris Nasus Larynx* 28:121–124, 2001.
[17] Lecamwasam, H. S., M. P. Sullivan, S. V. Yalla, and E. G. Cravalho. The flow regimes and the pressure-flow relationship in the canine urethra. *Neurourol. Urodyn.* 18:521–541, 1999.
[18] Liu, B. Y., and D. L. Tang. A numerical simulation of viscous flows in collapsible tubes with stenoses. *Appl. Numer. Math.* 32:87–101, 2000.
[19] Luo, X. Y., and T. J. Pedley. Multiple solutions and flow limitation in collapsible channel flows. *J. Fluid Mech.* 420:301–324, 2000.
[20] Matsuzaki, Y., T. Ikeda, T. Kitagawa, and S. Sakata. Analysis of flow in a two-dimensional collapsible channel using universal tube law. *J. Biomech. Eng.* 116:469–476, 1994.
[21] Miura, M., H. Takahashi, I. Honjo, S. Hasebe, and M. Tanabe. Influence of the upper respiratory tract infection on tubal compliance in children with otitis media with effusion. *Acta Oto-Laryngol.* 117:574–577, 1997.
[22] Miura, M., H. Takahashi, T. Sugimaru, and I. Honjo. Influence of surface condition of mucosa of eustachian tube on tubal compliance. *Acta Oto-Laryngol.* 116:840–844, 1996.
[23] Pedley, T. J., and X. Y. Luo. Modeling flow and oscillations in collapsible tubes. *Theor. Comput. Fluid Dyn.* 10:277–294, 1998.
[24] Sakakihara, J., I. Honjo, A. Fujita, K. Kurata, and H. Takahashi. Compliance of the patulous eustachian tube. *Ann. Otol. Rhinol. Laryngol.* 102:110–112, 1993.
[25] Sakakihara, J., I. Honjo, A. Fujita, K. Kurata, and H. Takahashi. Eustachian tube compliance in sniff-induced otitis media with effusion. A preliminary study. *Acta Oto-Laryngol.* 113:187–190, 1993.
[26] Schappert, S. M. Office visits for otitis media, United States 1975–1990. Vital and Health Statistics of the Centers for Disease Control/National Center for Health Statistics. 214, 1992.
[27] Suzuki, C., C. Balaban, I. Sando, M. Sudo, T. Ganbo, and M. Kitagawa. Postnatal development of Eustachian tube: A computer-aided 3D reconstruction and measurement study. *Acta Oto-Laryngol.* 118:837–843, 1998.
[28] Swarts, J. D., and S. R. Rood. The morphometry and three-dimensional structure of the adult eustachian tube: Implications for function. *Cleft Palate J.* 27:374–381, 1990.
[29] Takahashi, H., M. Hayashi, and I. Honjo. Compliance of the eustachian tube in patients with otitis media with effusion. *Am. J. Otolaryngol.* 8:154–156, 1987.
[30] Takahashi, H., I. Honjo, and A. Fujita. Eustachian tube compliance in cleft palate—A preliminary study. *Laryngoscope* 104:83–86, 1994.
[31] Tang, D., J. Yang, C. Yang, and D. N. Ku. A nonlinear axisymmetric model with fluid-wall interactions for steady viscous flow in stenotic elastic tubes. *J. Biomech. Eng.* 121:494–501, 1999.
[32] Teele, D. W., J. O. Klein, and B. Rosner. Epidemiology of otitis media during the first seven years of life in children in greater Boston: A prospective, cohort study. *J. Infect. Dis.* 160:83–94, 1989.
[33] Visual Numerics Inc. IMSL Fortran 90 MP Library. Houston, TX, 1997.
[34] White, F. M. Viscous flow in ducts. In: Fluid Mechanics, edited by J. J. Corrigan and D. A. Damstra. New York: McGraw-Hill, 1994.